Journal of Applied Polymer Science

Transparent and conductive indium tin oxide/polyimide films prepared by high-temperature radio-frequency magnetron sputtering

Yu Wen, Huan Liu, Shiyong Yang, Lin Fan

Laboratory of Advanced Polymer Materials, Institute of Chemistry, Chinese Academy of Sciences, Zhongguancun Beijing 100190, People's Republic of China

Correspondence to: L. Fan (Email: fanlin@iccas.ac.cn)

ABSTRACT: A highly transparent and thermally stable polyimide (PI) substrate was prepared and used for the fabrication of indium tin oxide (ITO)/PI films via radio-frequency magnetron sputtering at an elevated substrate temperature. The effect of the deposition conditions, that is, the oxygen flow rate, substrate temperature, sputtering power, and working pressure, on the optical and electrical properties of the ITO/PI films were investigated from the microstructural aspects. The results indicate that the optical and electrical properties of ITO were sensitive to the oxygen. Moreover, it was beneficial to the improvement of the ITO conductivity through the adoption of a high substrate temperature and sputtering power and a low working pressure in the deposition process. A two-step deposition method was developed in which a thick bulk ITO layer was overlapped by deposition on a thin seed ITO layer with a dense surface to prepare the highly transparent and conductive ITO/PI films. The ITO/PI film after annealing at 240°C gave a transmittance of 83% and a sheet resistance of 19.7 Ω/square. © 2015 Wiley Periodicals, Inc. J. Appl. Polym. Sci. **2015**, *132*, 42753.

KEYWORDS: films; optical and photovoltaic applications; polyimides

Received 17 May 2015; accepted 18 July 2015

DOI: 10.1002/app.42753

INTRODUCTION

In recent years, flexible electronics, such as rollable and bendable liquid-crystal displays, organic light-emitting diodes, and thin solar-film panels, have received much attention because of their potential for the fabrication of lightweight and ultrathin devices.[1,2] Many efforts have been made to develop transparent and conductive indium tin oxide (ITO) electrodes deposited on flexible polymeric substrates for use in place of conventional glass substrates for flexible electronics applications.[3–5] Flexible polymeric substrates are very promising materials for flexible devices with advantages of transparency, light weight, flexibility, robustness, low cost, and suitability for mass production via roll-to-roll processes.[1] However, the deposition of ITO on polymeric substrates presents challenges in optical and electrical integrity. High-quality ITO on a glass substrate is deposited at a substrate temperature of 300–400°C or first sputtered on the cold substrate and then annealed at 200°C in a controlled oxygen environment.[6] Commercially available transparent polymeric substrates, such as poly(ethylene terephthalate), poly(ethylene naphthalate), polycarbonate, and poly(ether sulfone), can only endure ITO deposition at temperatures lower than 150°C because of their low thermal stability. ITO deposited at low temperatures generally creates an amorphous ITO phase, and this results in poor conductivity.[7–9]

Polyimides (PIs) are well recognized as high-performance polymers because of their high thermal stability, good mechanical properties, and excellent chemical resistance; these make them good candidates for microelectronics applications. However, PIs have limited applications as flexible substrates in optoelectronics because of their certain color and difficult solubility.[10,11] In the past decade, many studies have been done on the development of highly optical transparent and colorless PIs.[12,13] In our previous study, a series of semiaromatic PIs were successfully prepared on the basis of fluorinated aromatic diamines and alicyclic dianhydrides.[14] These PIs exhibited excellent solubility, high thermal stability, and good mechanical properties combined with considerably improved optical transparency compared with conventional PIs. They gave glass-transition temperatures over 300°C and showed transmittances higher than 90% in the visible range; this made them good candidates for flexible substrates. We considered that highly transparent and thermally stable PIs could ensure the deposition of the ITO layer at an elevated substrate temperature and could further provide better ITO conductivity.

ITO has been prepared by various techniques, such as pulsed laser deposition,[15] radio-frequency (RF) magnetron sputtering,[16] the sol–gel method,[17] and electron beam evaporation.[18] Among these techniques, RF magnetron sputtering is widely used because it is considered to be one of the best methods for

© 2015 Wiley Periodicals, Inc.

preparing ITO with high quality in larger scale.[19,20] In the case of RF magnetron sputtering, the characterization of ITO layers is significantly dependent on the sputtering conditions, such as the oxygen flow rate, substrate temperature, sputtering power, and working pressure.[21–23] Many studies have been carried out on this field to optimize the deposition conditions and achieve the optimal performance of ITO layers. However, to our knowledge, very few attempts have been carried out to deposit ITO on PI substrates. Lim *et al.*[24] deposited ITO layers on the aliphatic cyclic PI substrate at different deposition temperatures with an RF magnetron sputtering system. They found that the sheet resistance of the ITO/PI film decreased with increasing substrate temperature; it was down to 34.6 Ω/square when the temperature was set at 150°C. However, the transmittance of the ITO/PI film was lower than 40% at a wavelength of 500 nm. Lozano *et al.*[25] prepared three kinds of aromatic PI substrates and fabricated ITO/PI films via RF magnetron sputtering at room temperature followed by vacuum annealing at temperatures of up to 400°C. They pointed out that the annealing treatment was effective for improving the conductivity. The results indicate that the resistivity of the ITO/PI film decreased from 1.5 to 0.8 mΩ·cm after annealing at 350°C, mainly because of the increment in the carrier concentration, wheareas the average transmittance was damaged with a drop to 75%. The Kapton films were also used as flexible substrates to deposit ITO layers by RF magnetron sputtering at room temperature. The influence of the oxygen partial pressure on the optical and electrical properties of the ITO/PI films was studied by Muneshwar *et al.*[26] They observed that the bulk carrier concentration decreased with increasing oxygen partial pressure during sputtering because the concentration of oxygen vacancies decreased. The ITO film with an 82% transmittance and minimum resistivity of 8.2×10^{-4} Ω cm was achieved on Kaptons substrate at an oxygen partial pressure of 0.6%. It is worth mentioning that the electrical and optical properties of the flexible ITO/PI films exhibited a trade-off relationship in the previous cases. Most studies have focused on the improvement of the conductivity of the ITO/PI films by ITO deposition at an elevated substrate temperature. Studies have scarcely dealt with how the ITO deposition conditions affects both of transparency and conductivity of ITO/PI films.

In this study, transparent and colorless PI containing semiaromatic structures were prepared and used as flexible substrates for the fabrication of ITO/PI films via RF magnetron sputtering at elevated substrate temperatures. The effect of the deposition conditions, that is, the oxygen flow rate, substrate temperature, sputtering power, and working pressure, on the optical and electrical properties of the ITO layers were investigated and are discussed in detail from the microstructure perspective. Moreover, a two-step ITO deposition method was developed to prepare ITO/PI films with a high transparency and conductivity. The influence of the heat treatment on the electrical properties of the ITO/PI films was also examined.

EXPERIMENTAL

Materials

1,2,4,5-Cyclohexanetetracarboxylic dianhydride (CHDA; TCI) was dried in a vacuum oven at 160°C for 12 h before use. 2,2′-

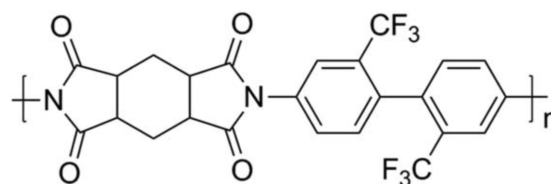

Scheme 1. Chemical structure of the PI film.

Bistrifluoromethyl-4,4′-diaminobiphenyl (TFDB; Changzhou Sunlight Fine Chemicals Co., China) was purified by recrystallization from ethanol or 2-methoxyethanol. *N,N*-Dimethylacetamide (DMAc) (Beihua Fine Chemicals Co., China) was purified by vacuum distillation and dehydrated with 4-Å molecular sieves before use. Toluene, ethanol, acetone, and other regents were used as received.

Preparation of the PI Substrate

PI was synthesized from the alicyclic dianhydride CHDA and the aromatic diamine TFDB via a one-pot solution polycondensation at high temperature in DMAc according to a method reported previously.[14] The chemical structure of the PI is shown in Scheme 1. In the reaction procedure, the TFDB (16.01 g, 0.05 mol) was dissolved in anhydrous DMAc; this was followed by the addition of CHDA (11.21 g, 0.05 mol), isoquinoline (0.3 g), and toluene (30 mL). The reaction solution was stirred in nitrogen at room temperature for 24 h and was then heated to 160°C and kept at that temperature for 12 h to complete the imidization. The fiberlike PI resin was obtained after the viscous reaction solution was poured into excess ethanol; this was followed by filtration, washing, and drying *in vacuo* in sequence. The number-average molecular weight of the PI resin determined by tandem gel permeation chromatography/multi-angle laser light scattering) was 4.6×10^4 g/mol. The PI resin was then dissolved in DMAc to get a homogeneous solution with a solid content of 30 wt %, and this solution was filtered by a 0.2-mm Teflon syringe filter. The free-standing PI substrate was obtained by the casting of the PI solution onto a glass plate; this was followed by thermal baking at conditions of 50°C for 15 min, 80°C for 1 h, 120°C for 1 h, 150°C for 1 h, and 160°C for 1 h.

Preparation of the ITO/PI Films

The ITO/PI films were prepared by the deposition of the ITO thin layers on PI substrates via RF magnetron sputtering. The ITO ceramic target with an In_2O_3/SnO_2 composition of 90:10 wt % and 99.99% purity ($\Phi = 80 \times 5$ mm). The flexible PI substrates with dimensions of 5×5 cm^2 were used, and they were ultrasonically cleaned with ethanol and deionized water to remove surface contamination. The distance between the target and the PI substrate was fixed at 75 mm. The vacuum chamber was evacuated to a background pressure of around 7.0×10^{-4} Pa; then, the PI substrate was heated to the elevated temperature before deposition. After that, the argon or the argon/oxygen mixture was introduced into the chamber until the required pressure was reached. To clarify the effect of the ITO deposition conditions on the optical and electrical properties of the ITO/PI films, the oxygen flow rate was changed from 0 to 6 sccm in the sputtering procedure. Moreover, the samples were also

prepared with a fixed oxygen flow rate of 2 sccm but with various substrate temperatures, sputtering powers, and working pressures in the ranges 120–260°C, 50–90 W, and 0.3–1.1 Pa, respectively. The thickness of the ITO layers was around 200 nm.

Measurements

The thermal properties of the PI substrate were evaluated by differential scanning calorimetry and thermogravimetric analysis, which were carried out with TA Q100 and TA Q50 instruments, respectively, at a heating rate of 10°C/min in nitrogen. The in-plane coefficient of thermal expansion (CTE) measurement of the PI substrate was recorded on a TA Q400 instrument in nitrogen and determined by the calculation of the result in the temperature range 50–200°C. The optical transmittance of the PI and ITO/PI films was recorded on a Shimadzu UV-2600 spectrophotometer at wavelengths of 280–800 nm. The color intensity of the ITO/PI films was evaluated by an X-Rite Color i7 spectrophotometer with an observational angle of 8° and a Commission International de l'Eclairage (CIE) standard D65 illuminant. A CIELAB color difference equation was used. X-ray photoelectron spectroscopy (XPS) was carried out with an ESCALab 220I-XL instrument with an Al Kα source. The binding energies were referenced to the C1s line at 284.8 eV from the adventitious carbon. The X-ray diffraction (XRD) measurements were conducted on a Rigaku D/max-2500 X-ray diffractometer with Cu Kα radiation and operated at 40 kV and 200 mA at a scanning speed of 3°/min. Scanning electron microscopy (SEM) was performed on a Hitachi S-4800 scanning electron microscope with film samples coated with platinum. Atomic force microscopy (AFM) was recorded on a Bruker multimode Nanoscope V in the tapping mode. The sheet resistance was measured with a four-point probe meter. The electrical properties, such as the resistivity, carrier concentration, and mobility of the ITO/PI films were determined by a Phystech RH2030 Hall-effect measurement system at room temperature with the van der Pauw method.

RESULTS AND DISCUSSION

Characterization of the PI Substrate

The flexible and highly transparent PI substrate with good thermal stability was successfully prepared from PI derived from the alicyclic dianhydride CHDA and the aromatic diamine TFDB via a one-pot solution polycondensation at high temperature. The PI substrate with a thickness of 50 μm exhibited transmittances in the range 400–800 nm over 94% combined with a UV absorption edge lower than 300 nm, as shown in Figure 1. The optical transparency of the PI substrate was also evaluated by the color intensities from the lightness (L^*), redness (a^*), and yellowness (b^*) indices detected by a color-eye colorimeter. The PI film showed a high L^* with an L^* value over 96 and exhibited nearly a zero a^* value combined with an extremely low b^* value of 0.15. This indicated an extremely transparent and essentially colorless PI substrate. The PI substrate exhibited good thermal stability with a glass-transition temperature of 370°C and a decomposition temperature at 5% weight loss of 474°C, respectively; this was superior to most commercially available colorless and transparent polymer films, as mentioned previously. We also noticed that the PI substrate revealed an extremely low CTE of 35 ppm/°C because of the presence of a rigid biphenyl unit in the main chain. The excellent thermal stability and low CTE of the PI substrate can ensure the deposition of the ITO layer at elevated substrate temperatures and can further provide better ITO conductivity.

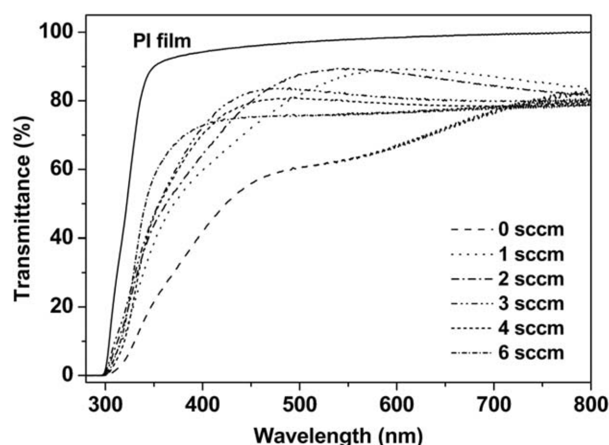

Figure 1. Transmittance spectra of the PI and ITO/PI films prepared with various oxygen flow rates.

Optical and Electrical Properties of the ITO/PI Films

The optical and electrical properties of the ITO layers strongly depended on their structural characteristics, such as the oxygen vacancy, activation of tin dopant, and crystallinity and compactness; these correlated with the preparation conditions. Therefore, the effects of the deposition conditions on the optical and electrical properties of the ITO layers were investigated from the microstructure perspective with an aim to develop highly transparent and conductive ITO/PI films.

Effect of the Oxygen Flow Rate on the Optical and Electrical Properties. It is known that oxygen gas plays a crucial role in controlling the optical properties of ITO layers. An increase in oxygen in ITO close to the stoichiometric compound will decrease the defects and lead to better optical properties. However, the incorporation of oxygen will decrease the electrical conductivity simultaneously. The ITO/PI films were prepared by the deposition of ITO layers with various oxygen flow rates at a constant PI substrate temperature of 180°C with a sputtering power of 70 W and a working pressure of 0.8 Pa. The thicknesses of the ITO layers was around 100 nm.

The transmittance spectra of the ITO/PI films prepared with different oxygen flow rates are shown in Figure 1, and the corresponding average transmittances in the visible light region (400–800 nm) are listed in Table I. The transmittances of the ITO/PI films were lower than those of the PI substrate. The average transmittances of these ITO/PI films in the visible-light region displayed an initial increasing followed by a decrease along with the increase in the oxygen flow rate. The ITO/PI film prepared with the moderate oxygen flow rate of 2 sccm gave the highest transmittance of 84.1%. We considered that the nonstoichiometric compounds, that is, suboxides of InO_x and SnO_x, were dominated in the ITO layer at an oxygen flow rate

Table I. Average Transmittance and Color Coordinates of the ITO/PI Films Prepared with Various Oxygen Flow Rates

Oxygen flow rate (sccm)	T_{av} (%)[a]	L^*	a^*	b^*
0	67.3	84.55	1.57	9.30
1	82.9	95.16	−1.54	10.42
2	84.1	95.58	−3.24	5.80
3	80.8	95.45	−2.59	4.76
4	78.8	94.94	−1.16	1.65
6	76.8	92.28	0.18	0.48

The color parameters were calculated according to a CIELAB equation. For the L^* values, 100 means white, whereas 0 indicates black. A positive a^* value means red, whereas a negative a^* value indicates green. A positive b^* value means yellow, whereas a negative b^* value indicates blue.
[a] Average transmittance of the ITO/PI films in the range 400–800 nm.

lower than 2 sccm; this resulted in the absorption and scattering in the visible spectra. However, when the oxygen flow rate was over 2 sccm, the redundant oxygen might have been absorbed in the defects; these included the grain boundary and microcracks, which acted as light-scattering centers and caused a decrease in the transmittance of the ITO/PI film.[27] The optical performance of these ITO/PI films was also evaluated by the color intensities from L^*, a^*, and b^* indices detected by a color-eye colorimeter. As illustrated in Table I, both the L^* and b^* values exhibited increases followed by decreases with increasing oxygen flow rate; this was consistent with the changing trend of the average transmittances. For the ITO/PI films prepared with oxygen flow rates lower than 2 sccm, the relatively higher b^* values suggested the yellow to brown coloration of films was due to the existence of suboxides. On the other hand, for the ITO/PI films prepared with oxygen flow rates higher than 2 sccm, the L^* and b^* values showed decreases with the further introduction of oxygen because of excessive oxidation. The extremely transparent and essentially colorless ITO/PI film was obtained as the oxygen flow rate was set at 2 sccm; these displayed the highest L^* values combined with a relatively low b^* value as compared with the others.

The oxygen flow rate also significantly affected the electrical properties of the ITO/PI films because the doubly charged oxygen vacancies acted as donors in the ITO layers. As shown in Table II, the sheet resistance of the ITO/PI films prepared without oxygen was as low as 0.05 kΩ/square, whereas it increased abruptly with increasing oxygen flow rate. The ITO/PI film prepared with an oxygen flow rate of 6 sccm gave an extremely high sheet resistance of 372.4 kΩ/s. This was correlated with an oxygen vacancy concentration and oxygen states in the ITO layers. Figure 2 shows the O1s XPS spectra of the ITO layers prepared with various oxygen flow rates. The O1s spectra could be fitted with three components around 529.9, 531.5, and 533.0 eV (referred to as O_I, O_{II}, and O_{III}, respectively) with three Gaussian functions with variable positions, widths, and intensities. The O_I and O_{II} peaks came from the In_2O_3 region and the oxygen-deficient region, respectively.[28] The O_I component was attributed to the O^{2-} ions in the In_2O_3 region, which had neighboring indium atoms with a full complement of six nearest neighbor O^{2-} ions. The O_{II} component was related to the O^{2-} ions in the oxygen-deficient region without neighboring indium atoms. The O_{III} component may have originated from organic oxygen contamination, probably in the form of carboxyl groups, because a broad peak of C1s was located in the range of 286.5–289.0 eV (not shown in the article).[29] The relative strengths were obtained by a comparison of the integrated areas of the O_I and O_{II} components. As illustrated in Table II, the ratios of O_I/O_{II} became larger as more oxygen was added during sputtering; this suggested fewer oxygen vacancies in the ITO layers and resulted in a decrease in the conductivity.

The XRD patterns of the ITO/PI films prepared at different oxygen flow rates are displayed in Figure 3. The relatively strong (400) peak combined with weak (222), (440), and (622) peaks were detected; this was consistent with the standard diffraction peaks of In_2O_3. We also observed that the ITO layer prepared without oxygen exhibited a sharp (400) plane; this implied the well-ordered crystalline. However, the intensity of the (400) plane decreased with increasing oxygen flow rate. This suggested the reduction of the crystallinity of the ITO layer. Moreover, from the SEM micrographs of the ITO surface, we observed that the ITO layer prepared without oxygen exhibited a relatively smoother surface than the others. The ITO surface became rougher when the oxygen flow rate increased; this was caused by the increase in the number of the grain boundaries and the decrease in grain sizes.[30] It is known that an electron carrier can conduct more quickly in a well-ordered crystalline structure. Therefore, the ITO/PI film prepared without oxygen revealed a lower sheet resistance because of its higher crystallinity. The increases in the sheet resistance of the ITO layers along with the incorporation of oxygen was related to their rough surface. Under the comprehensive consideration of the influence of oxygen flow rate on the optical and electrical properties of the ITO/PI films, we concluded that the ITO layer prepared with a moderate oxygen flow rate of 2 sccm could result in ITO/PI films with a good balance of optical and electrical properties. Therefore, the oxygen flow rate was set at 2 sccm in the following research.

Effect of the Substrate Temperature on the Electrical Properties. ITO layers deposited at substrate temperatures higher than 150°C generally exhibit a polycrystalline structure

Table II. Sheet Resistances of the ITO/PI Films Prepared with Various Oxygen Flow Rates and Oxygen States of the Corresponding ITO Layers

Oxygen flow rate (sccm)	Sheet resistance (kΩ/square)	Position (eV)		O_I/O_{II} peak ratio
		O_I	O_{II}	
0	0.05	529.9	531.5	0.34
1	14.7	529.8	531.6	0.57
2	31.7	529.8	531.6	0.67
3	147.2	529.9	531.6	0.72
4	226.1	529.9	531.5	0.75
6	372.4	530.0	531.6	0.82

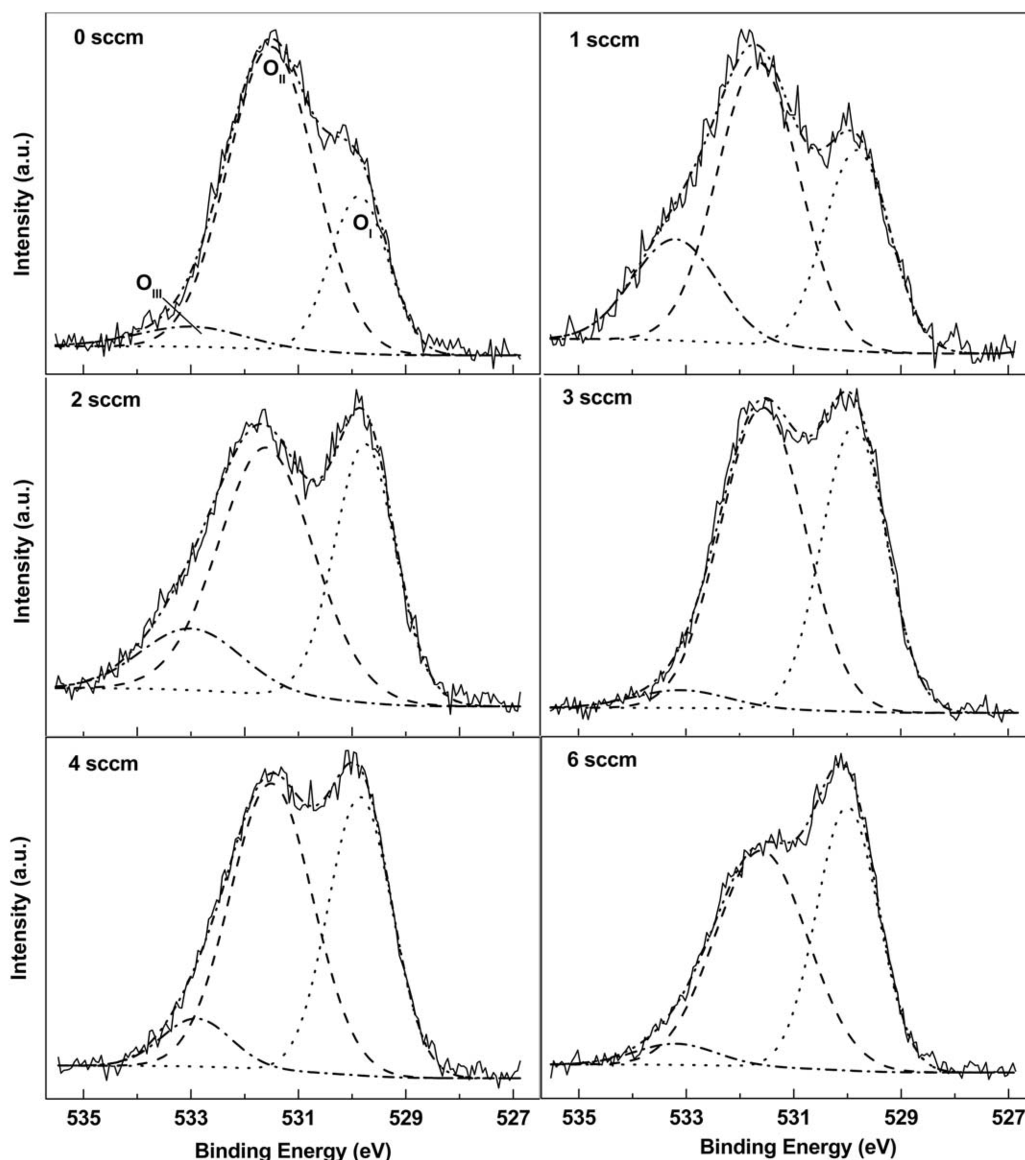

Figure 2. O1s XPS spectra of the ITO layers prepared with various oxygen flow rates.

with different orientation distribution of the crystalline grains; this significantly affects their electrical properties.[31] The highly thermally stable PI film prepared in this research afforded the deposition of ITO layers at an elevated temperature. Therefore, the ITO/PI films were fabricated at substrate temperatures that varied from 120 to 260°C with a constant oxygen flow rate of 2 sccm, a sputtering power of 70 W, and a working pressure of 0.8 Pa. As shown in Figure 4, the sheet resistances of the ITO/PI films dramatically dropped from 156.1 to 8.3 kΩ/square when the substrate temperature was raised from 120 to 220°C, and no obvious change was detected as the substrate temperature further increased to 260°C.

The effect of the substrate temperature on the electrical properties of the ITO/PI films could be explained in terms of the crystallinity and the grain size of ITO. The XRD patterns of the ITO layers deposited at different substrate temperatures are shown in Figure 5. The diffraction peaks of ITO due to the (222), (400), (440), and (622) planes were detected for the ITO layers deposited at temperatures of 120 and 180°C, whereas the (222) peak disappeared, and the (400) peak became sharper as the substrate temperature increased up to 260°C; this indicated an improvement in the crystallinity of the ITO layers. It has been reported that the adatoms on substrate have sufficient energy at high temperature, which favor to grow the ITO layer along the (400) orientations to form crystalline with large grains.[32] The better crystallinity of ITO may reduce the grain boundary scattering and increase the carrier mobility, as a result, leading to the decrease of sheet resistance.[33,34] We also observed that there were almost no changes in color and shape compared to the films before and after ITO deposition at temperatures of no more than 220°C. However, the ITO/PI film deposited at substrate temperatures as high as 260°C revealed a slight warp due to the shrinking of the PI substrate.

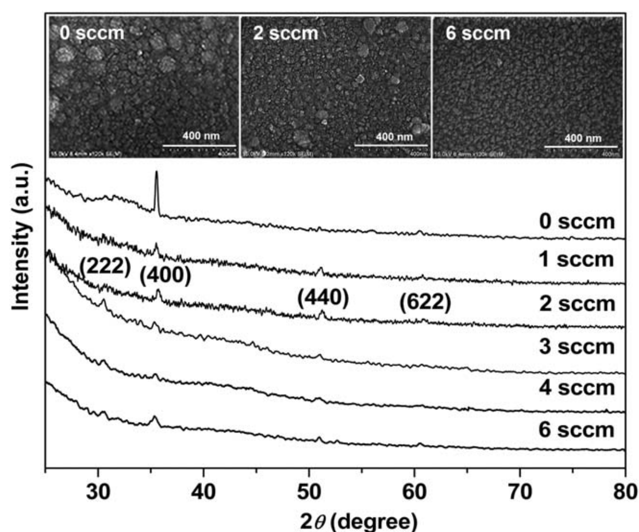

Figure 3. XRD patterns of the ITO layers prepared with various oxygen flow rates. The insets show the SEM micrographs of the ITO surface.

Effect of the Sputtering Power on the Electrical Properties. The sputtering power was one of the most important factors influencing the properties of the ITO layers. The ITO/PI films were prepared with various sputtering powers at a constant oxygen flow rate of 2 sccm, a substrate temperature of 220°C, and a working pressure of 0.8 Pa. We found that the ITO layer prepared with the relatively higher sputtering power gave better electrical properties. As listed in Table III, the sheet resistance of the ITO/PI film prepared at a sputtering power of 90 W was only 6.5 kΩ/square; this was an order of magnitude lower than the film prepared at a sputtering power of 50 W. A theoretically high sputtering power will generate more argon ions and then sputter more Sn^{4+}.[35] The effective doping of Sn^{4+} can lead to a higher carrier density and decrease the resistivity.[36] Figure 6 shows the Sn $3d_{5/2}$ XPS spectra of the ITO layers prepared with various sputtering powers. The asymmetrical Sn $3d_{5/2}$ peaks indicated the existence of multiple components, which could be resolved into two peaks centered at 486.2 and 487.1 eV and due to the oxidation states of Sn^{2+} and Sn^{4+}, respectively.[37] The ratios of Sn^{4+}/Sn^{2+} were calculated from the corresponding integrated areas and are listed in Table III. The ratio of Sn^{4+}/Sn^{2+} increased from 0.76 to 0.98 with increasing sputtering power; this suggested an increase in the concentration of Sn^{4+}. Moreover, according to the XRD patterns of the ITO layers prepared with various sputtering powers, we also found that the (400) interplanar spacing calculated from the Bragg formula increased from 2.5252 to 2.5363 Å with increasing sputtering power; this inferred that the lattice constant expanded from 10.1008 to 10.1452 Å. The expansion of the lattice could be explained in terms of the replacement of In^{3+} by Sn^{4+} because the lattice constant of SnO_2 (10.330 Å) was larger than that of In_2O_3 (10.118Å).[38] Therefore, we confirmed that the relatively higher sputtering powers used for the ITO/PI films were beneficial for gaining ITO layers with higher Sn^{4+} concentrations and resulted in a decrease in the sheet resistance.

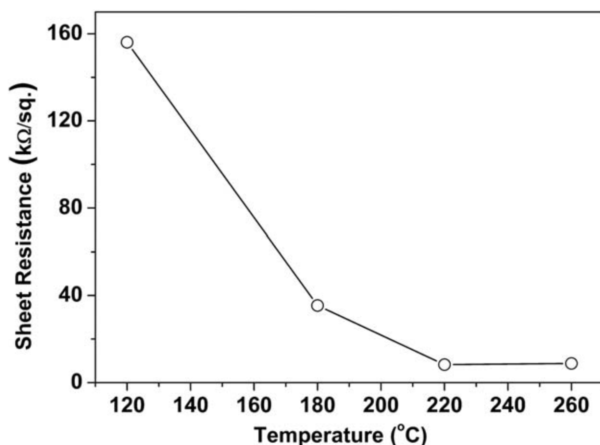

Figure 4. Variation of the sheet resistance of the ITO layers deposited at different substrate temperatures.

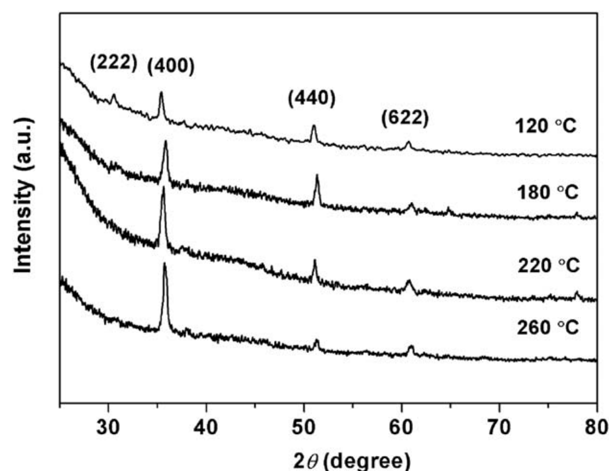

Figure 5. XRD patterns of the ITO layers deposited at different substrate temperatures.

Effect of the Working Pressure on the Electrical Properties. The electrical properties of the ITO layers was also significantly affected by the working pressure in the sputtering process. The ITO/PI films were prepared under a working pressure that varied from 0.3 to 1.1 Pa in a pure argon atmosphere to exclude the influence of the oxygen flow rate. Moreover, the substrate temperature and sputtering power were set at 220°C and 90 W, respectively. The resistivity and carrier mobility of these ITO/PI films were determined by the Hall-effect measurement and are shown in Figure 7. The ITO/PI films had a resistivity of higher than 20×10^{-4} Ω cm when the ITO layers were

Table III. Sheet Resistance of the ITO/PI Films Prepared with Various Sputtering Powers and Sn States and Crystal Parameters of the Corresponding ITO Layers

Sputtering power (W)	Sheet resistance (kΩ/square)	Sn^{4+}/Sn^{2+}	Interplanar spacing (Å)	Lattice constant (Å)
50	64.2	0.76	2.5252	10.1008
70	8.3	0.83	2.5349	10.1396
90	6.5	0.98	2.5363	10.1452

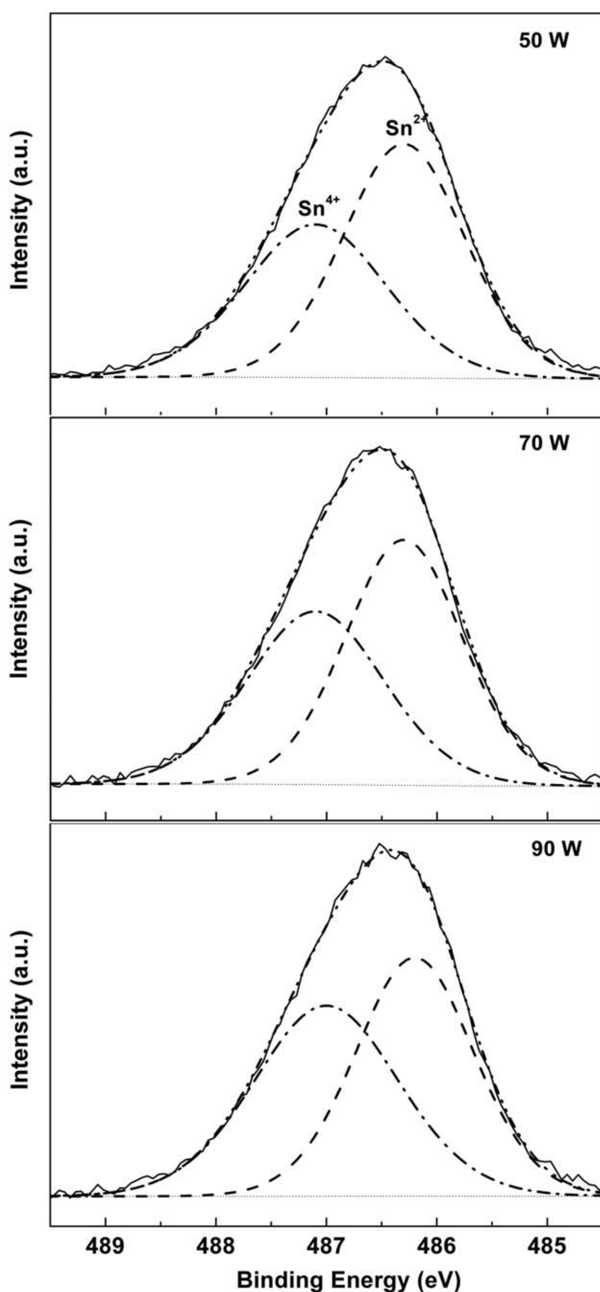

Figure 6. Sn $3d_{5/2}$ XPS spectra of the ITO layers prepared with various sputtering powers.

prepared under a working pressure of 0.8–1.1 Pa, whereas the resistivity abruptly decreased to 3.48×10^{-4} and 2.09×10^{-4} Ω cm when the working pressures were as low as 0.5 and 0.3 Pa, respectively. Meanwhile, the carrier mobility of the ITO/PI films increased from 0.43 to 2.34 cm^2/Vs as the working pressure decreased. It has been reported that ITO layers prepared at lower working pressures tend to grow a uniform grain, and this leads to a dense surface.[16] The surface roughness could be a barometer for the crystalline quality; this was determined by AFM, and the image is also displayed in Figure 7. The results indicate that the ITO layer prepared at a working pressure of 1.1 Pa gave a surface roughness of 1.97 nm, which decreased to

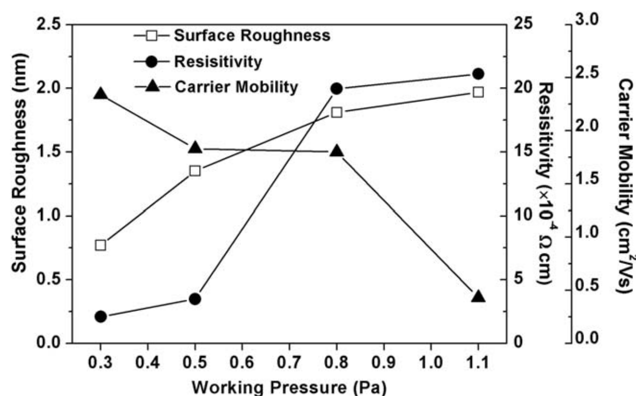

Figure 7. Resistivity, carrier mobility, and surface roughness of the ITO/PI films as a function of the working pressure.

0.77 nm for the ITO prepared at a working pressure of 0.3 Pa. We considered that the lower surface roughness was related to the lower lattice distortion; this resulted in a reduction of electron scattering and a higher carrier mobility.

Transparent and Conductive ITO/PI Films

According to the effects of the deposition conditions on the optical and electrical properties of the ITO/PI films discussed previously, we clarified that adopting the high substrate temperature and sputtering power and the low working pressure in a pure argon atmosphere during the deposition process was beneficial for improving the conductivity of the ITO layer. However, the ITO/PI films prepared without oxygen led to poor transparency because of the existence of suboxides. We also confirmed that the conductivity of the ITO layer was strongly dependent on the crystallinity, and this was closely related to the degree of lattice distortion of the ITO crystal. It has been reported that the crystalline quality and preferential orientation of ITO strongly depends on the initial stage of deposition.[39,40]

On the basis of the previous point of view, we tried to prepare ITO/PI films with high conductivities and good transparencies

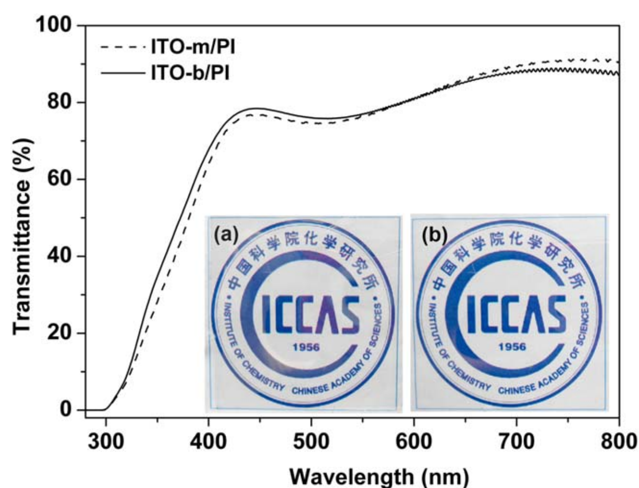

Figure 8. Transmittance spectra of the ITO-m/PI and ITO-b/PI films. The insets show the photographs of the (a) ITO-m/PI and (b) ITO-b/PI films. [Color figure can be viewed in the online issue, which is available at wileyonlinelibrary.com.]

Table IV. Optical and Electrical Properties of the As-Deposited ITO-m/PI and ITO-b/PI Films and Annealed ITO-m/PI Film

Sample	T_{av} (%)[a]	b^*	Carrier concentration (cm^{-3})	Carrier mobility (cm^2/Vs)	Resistivity (Ω cm)	Sheet resistance (Ω/square)
ITO-m/PI	81.9	2.27	1.17×10^{19}	11.71	4.56×10^{-2}	2.3×10^{3}
ITO-b/PI	81.6	2.74	2.26×10^{20}	30.62	9.03×10^{-4}	45.2
Annealed ITO-b/PI	83.0	2.19	4.70×10^{21}	3.31	3.94×10^{-4}	19.7

[a] Average transmittance of the ITO/PI films in the range 400–800 nm.

via a two-step growth process. First, a thin ITO-s was deposited in a pure argon atmosphere at a substrate temperature of 220°C with a sputtering power of 90 W and a working pressure of 0.3 Pa; this was expected to grow ITO with a dense surface. Then, a thick bulk layer was deposited in mixed argon/oxygen gas at an oxygen flow rate of 2 sccm under a working pressure of 0.5 Pa with the same substrate temperature and sputtering power. We verified that the optical properties were sensitive to the oxygen flow rate. Therefore, the incorporation of oxygen in the second step was predicted to provide an ITO with good transparency. The thin ITO-s and the thick bulk layer of ITO had thicknesses of 40 and 160 nm, respectively. For comparison, the ITO/PI film was also prepared via a conventional one-step process with the same deposition conditions for the thick bulk layer of ITO except for the thickness of 200 nm. The ITO/PI films with bilayers and monolayers of ITO are referred to as ITO-b/PI and ITO-m/PI, respectively.

The optical properties of the ITO-m/PI and ITO-b/PI films were evaluated by their physical appearances, transmittance spectra, and color intensities. Figure 8 shows the transmittance spectra and photographs of these films. Both of the ITO-m/PI and ITO-b/PI films were highly transparent and entirely colorless. They gave average transmittances in the range 400–800 nm over 81% and values of b^* less than 3, as listed in Table IV. The electrical properties of these films were also evaluated by the Hall-effect measurement. As compared to ITO-m/PI and ITO-b/PI, we found that the latter exhibited a very low resistivity of 9.03×10^{-4} Ω cm, which was two orders of magnitude lower than that of the former. The difference in the conductivity between the ITO-m/PI and ITO-b/PI films could be explained from the surface morphology perspective. From the AFM three-dimensional (3D) images of these films shown in Figure 9, we observed that the ITO-m/PI showed a surface roughness of 4.73 nm, which was related to the lattice distortion to some extent. On the contrary, ITO-b/PI revealed a smoother morphology with a relatively lower surface roughness of 2.84 nm; this suggested a higher crystalline quality and denser surface morphology. The lower surface roughness of ITO-b/PI means that there was less lattice distortion and a reduced electron scattering of ITO compared to that in the ITO-m/PI. As a consequence, the former gave a carrier mobility of 30.62 cm^2/Vs, which was twice as much as that of the latter.

We suspect that the dense surface of the ITO-b/PI was due to the introduction of the initial ITO-s before the conventional one-step deposition of the ITO layer. The surface morphology of the seed ITO layer (defined as ITO-s) was investigated by AFM 3D and two-dimensional (2D) images as shown in Figure 10. For comparison, a thin ITO layer with thickness of 40 nm was also deposited with the same conditions as that for ITO-s except in mixed argon/oxygen gas with an oxygen flow rate of 2 sccm (defined as ITO-r). We observed that the ITO-s exhibited quite a smooth and dense surface with a very low surface roughness of 0.67 nm. On the other hand, ITO-r revealed an uneven surface with many defects and gave a high roughness of 2.21 nm. It is suggested that the ITO-s with a dense surface in

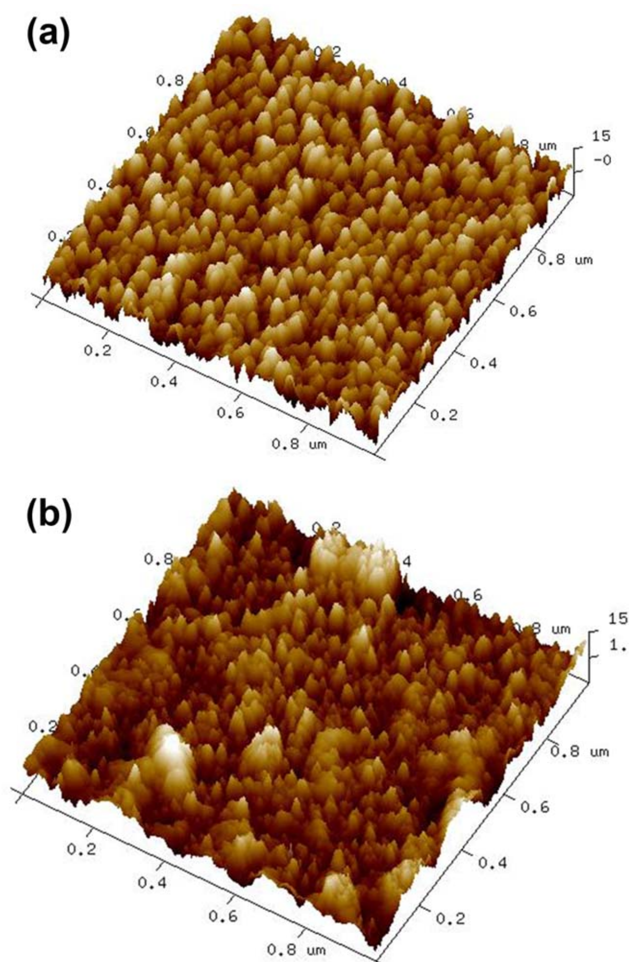

Figure 9. AFM 3D images of the (a) ITO-m/PI and (b) ITO-b/PI films. [Color figure can be viewed in the online issue, which is available at wileyonlinelibrary.com.]

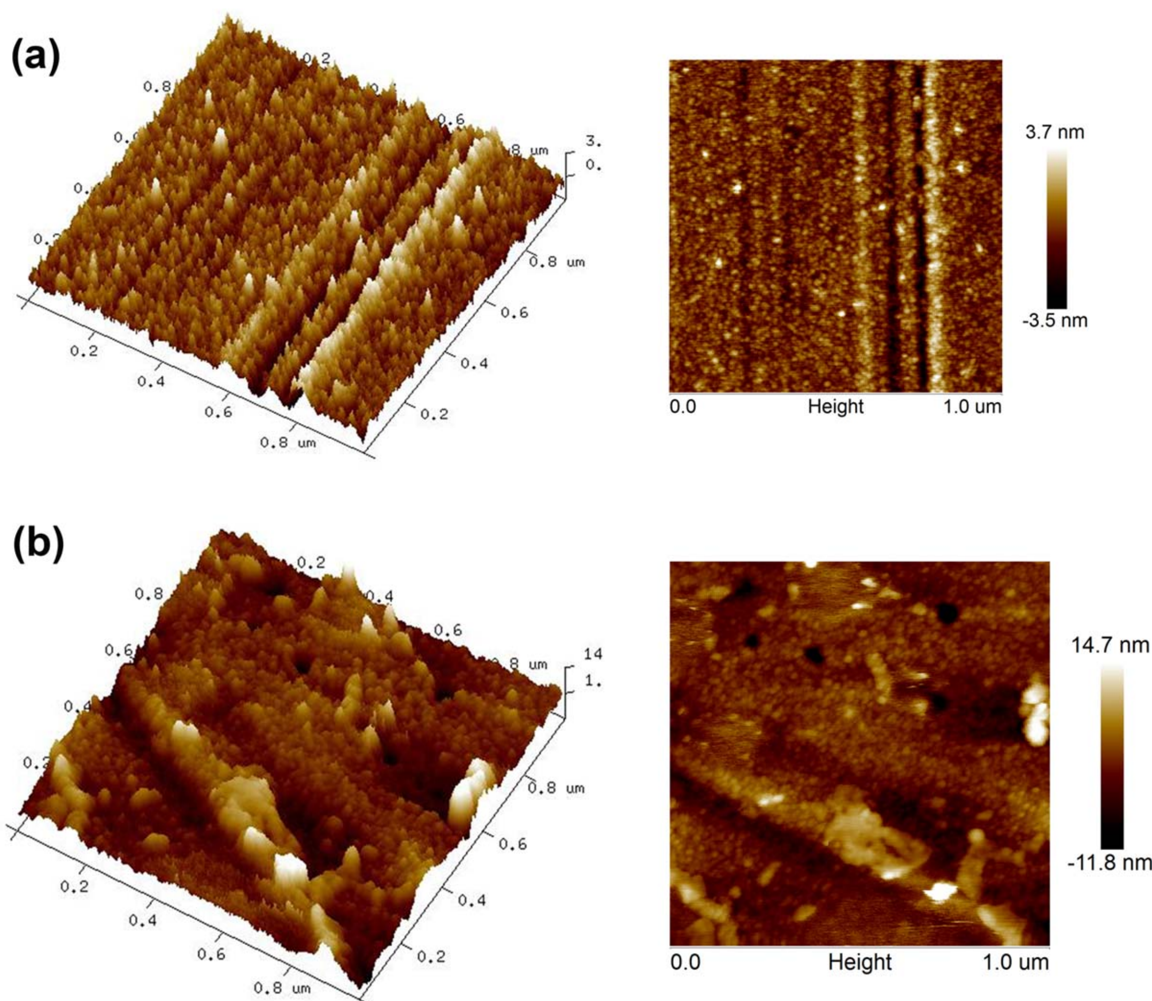

Figure 10. AFM 3D and 2D images of (a) ITO-s and (b) ITO-r (thickness = 40 nm). [Color figure can be viewed in the online issue, which is available at wileyonlinelibrary.com.]

the initial stage of deposition promoted the following ITO growth with a high crystalline quality and, hence, improved the conductivity of the ITO/PI film.

Heat treatment is effective in the modification of the structure, such as the structural defects, grain size, shape, and crystallinity, which plays an important role in the electrical properties of the ITO layers.[41,42] The ITO-b/PI film was subsequently annealed *in vacuo* at a temperature of 240°C to further improve the conductivity. In the annealing process, the temperature was enhanced slowly with a heating rate of 1°C/min to reduce the internal stress; this was followed by an isothermal treatment at 240°C for 30 min. From the XRD patterns shown in Figure 11, we found that the annealed ITO-b/PI exhibited relatively sharper (222) and (400) peaks compared to the as-deposited one; this suggested an improvement in the crystalline quality, as expected. This was also confirmed by the SEM micrographs of the corresponding ITO surfaces, in which the annealed ITO-b/PI showed more uniform and larger grains than the as-deposited one. The annealed film exhibited a much higher

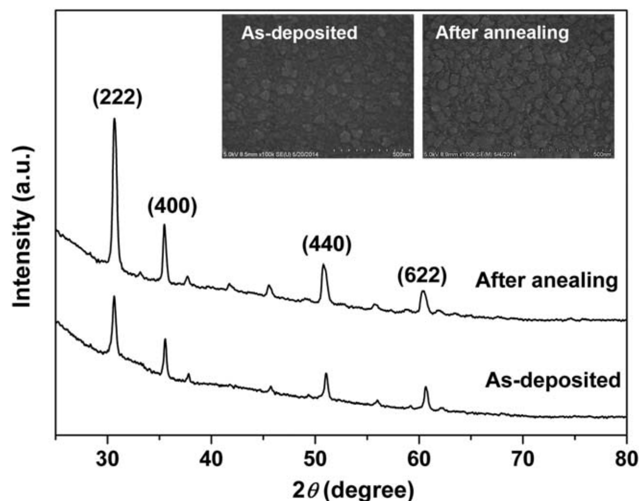

Figure 11. XRD patterns of the as-deposited and annealed ITO-b/PI films. The insets show the SEM micrographs of the corresponding ITO surfaces.

carrier concentration and lower resistivity than the as-deposited film. The excellent conductivity of the former was attributed to its better crystallinity. It is worth mentioning that the sheet resistance of the annealed ITO-b/PI film was as low as 19.7 Ω/square; this is comparable to the commercially available conductive ITO/poly(ethylene terephthalate) film.[43] Moreover, the average transmittance of the annealed ITO-b/PI film slightly increased to 83%; this was associated with a lower scattering effect, which was due to the reduced roughness and better crystallinity. In terms of the color intensity, the annealed ITO/PI film gave a relatively low b^* value of 2.19. The results indicate that the optical properties of the ITO-b/PI film was still maintained after heat treatment.

CONCLUSIONS

A highly transparent and thermally stable PI substrate was prepared from PI derived from the alicyclic dianhydride CHDA and the aromatic diamine TFDB by solution polycondensation at high temperature; this was used in the deposition of ITO layers to fabricate ITO/PI films via RF magnetron sputtering at elevated substrate temperatures. The correlation of the deposition conditions with the optical and electrical properties of the ITO layers were investigated from the microstructure perspective. The results suggest that both the electrical and optical properties, especially the color intensity, of the flexible ITO/PI films were sensitive to the oxygen flow rate during the sputtering process. We also confirmed that the adoption of the high substrate temperature and sputtering power and the low working pressure during the deposition process were beneficial to the improvement of the conductivity of the ITO layer. The highly transparent and conductive ITO-b/PI film was successfully prepared by a two-step ITO deposition process, in which a thick bulk ITO layer was overlapped in deposition on the thin ITO-s. The results demonstrate that the ITO-s with a dense surface in the initial stage of deposition could promote the following ITO growth with a highly crystalline quality and, as a consequence, could enhance the conductivity of the ITO/PI film. The heat treatment was effective in improving the electrical properties of the ITO/PI film. The ITO-b/PI film after annealing at 240°C gave a much higher carrier concentration and a relatively lower sheet resistance than the as-deposited film; this was due to the better crystallinity of the former.

ACKNOWLEDGMENTS

The authors gratefully acknowledge the financial support of the National Basic Research Program of China (contract grant number 2014CB643600).

REFERENCES

1. Choi, M.-C.; Kim, Y.; Ha, C.-S. *Prog. Polym. Sci.* **2008**, *33*, 581.
2. Logothetidis, S. *Mater. Sci. Eng. B* **2008**, *152*, 96.
3. Kim, D.-H.; Park, M.-R.; Lee, G.-H. *Surf. Coat. Technol.* **2006**, *201*, 927.
4. Carcia, P. F.; McLean, R. S.; Reilly, M. H.; Li, Z. G.; Pillione, L. J.; Messier, R. F. *J. Vacuum Sci. Technol. A* **2003**, *21*, 745.
5. Han, H.; Adams, D.; Mayer, J. W.; Alford, T. L. *J. Appl. Phys.* **2005**, *98*, 083705.
6. Wong, W. S.; Salleo, A. Flexible Electronics: Materials and Applications; Springer Science & Business Media: New York, **2009**; p 11.
7. Lan, Y. F.; Peng, W. C.; Lo, Y. H.; He, J. L. *Org. Electron.* **2010**, *11*, 670.
8. Tseng, K.-S.; Lo, Y.-L. *Appl. Surf. Sci.* **2013**, *285*, 157.
9. Shigesato, Y.; Koshi-Ishi, R.; Kawashima, T.; Ohsako, J. *Vacuum* **2000**, *59*, 614.
10. Ito, H.; Oka, W.; Goto, H.; Umeda, H. *Jpn. J. Appl. Phys.* **2006**, *45*, 4325.
11. MacDonald, W. A. *J. Mater. Chem.* **2004**, *14*, 4.
12. Zhang, W.; Xu, H.-J.; Yin, J.; Guo, X.-X.; Ye, Y.-F.; Fang, J.-H.; Sui, Y.; Zhu, Z.-K.; Wang, Z.-G. *J. Appl. Polym. Sci.* **2001**, *81*, 2814.
13. Mizoguchi, K.; Shibasaki, Y.; Ueda, M. *J. Photopolym. Sci. Technol.* **2007**, *20*, 181.
14. Zhai, L.; Yang, S.; Fan, L. *Polymer* **2012**, *53*, 3529.
15. Adurodija, F. O.; Semple, L.; Brüning, R. *J. Mater. Sci.* **2006**, *41*, 7096.
16. Patel, K. J.; Desai, M. S.; Panchal, C. J. *J. Mater. Sci. Mater. Electron.* **2011**, *22*, 959.
17. Kundu, S.; Biswas, P. K. *Chem. Phys. Lett.* **2005**, *414*, 107.
18. Xu, Z.; Chen, P.; Wu, Z.; Xu, F.; Yang, G.; Liu, B.; Tan, C.; Xu, Z.; Zhang, L.; Zhang, R.; Zheng, Y. *J. Mater. Sci. Mater. Electron.* **2014**, *25*, 2287.
19. Baia, I.; Quintela, M.; Mendes, L.; Nunes, P.; Martins, R. *Thin Solid Films* **1999**, *337*, 171.
20. Bräuer, G. *Surf. Coat. Technol.* **1999**, *112*, 358.
21. Malathy, V.; Sivaranjani, S.; Vidhya, V. S.; Balasubramanian, T.; Prince, J. J.; Sanjeeviraja, C.; Jayachandran, M. *J. Mater. Sci. Mater. Electron.* **2010**, *21*, 1299.
22. Meng, L.-J.; dos Santos, M. P. *Thin Solid Films* **1997**, *303*, 151.
23. Wu, W.-F.; Chiou, B.-S; Hsieh, S.-T. *Semicond. Sci. Technol.* **1994**, *9*, 1242.
24. Lim, H.; Bae, C. M.; Kim, Y. K.; Park, C. H.; Cho, W. J.; Ha, C. S. *Synth. Met.* **2003**, *135-136*, 49.
25. Lozano, A. E.; Abajo, J. D.; de la Campa, J. G.; Guillén, C.; Herrero, J.; Gutiérrez, M. T. *J. Appl. Polym. Sci.* **2007**, *103*, 3491.
26. Muneshwar, T. P.; Varma, V.; Meshram, N.; Soni, S.; Dusane, R. O. *Sol. Energy Mater. Sol. Cells* **2010**, *94*, 1448.
27. Houng, B.; Wang, A. *Appl. Surf. Sci.* **2012**, *258*, 5593.
28. Wu, W.-F.; Chiou, B.-S. *Semicond. Sci. Technol.* **1996**, *11*, 196.
29. Kim, J. S.; Ho, P. K. H.; Thomas, D. S.; Friend, R. H.; Cacialli, F.; Bao, G. W.; Li, S. F. Y. *Chem. Phys. Lett.* **1999**, *315*, 307.
30. Lee, H.-C.; Ok Park, O. *Vacuum* **2004**, *77*, 69.

31. Yi, C. H.; Yasui, I.; Shigesato, Y. *Jpn. J. Appl. Phys.* **1995**, *34*, 1638.
32. Meng, L. -J.; dos Santos, M. P. *Thin Solid Films* **1998**, *322*, 56.
33. Xu, J.; Yang, Z.; Wang, H.; Xu, H.; Zhang, X. *Mater. Sci. Semicond. Process.* **2014**, *21*, 104.
34. Nisha, M.; Anusha, S.; Antony, A.; Manoj, R.; Jayaraj, M. K. *Appl. Surf. Sci.* **2005**, *252*, 1430.
35. Matsuda, Y.; Yamori, Y.; Muta, M.; Ohgushi, S.; Fujiyama, H. *Jpn. J. Appl. Phys.* **1997**, *36*, 4922.
36. Terzini, E.; Thilakan, P.; Minarini, C. *Mater. Sci. Eng. B* **2000**, *77*, 110.
37. Nunes de Carvalho, C.; Botelho do Rego, A. M.; Amaral, A.; Brogueira, P.; Lavareda, G. *Surf. Coat. Technol.* **2000**, *124*, 70.
38. Akkad, F. E.; Marafi, M.; Punnoose, A.; Prabu, G. *Phys. Stat. Sol. A* **2000**, *177*, 445.
39. Kim, D.-H.; Park, M.-R.; Lee, H.-J.; Lee, G.-H. *Appl. Surf. Sci.* **2006**, *253*, 409.
40. Pham, D. P.; Phan, B. T.; Hoang, V. D.; Nguyen, H. T.; Ta, T. K. H.; Maenosono, S.; Tran, C. V. *Thin Solid Films A* **2014**, *570*, 16.
41. Zhu, G.; Yang, Z. *J. Mater. Sci. Mater. Electron.* **2013**, *24*, 3646.
42. Senol, S. D.; Senol, A.; Ozturk, O.; Erdem, M. *J. Mater. Sci. Mater. Electron.* **2014**, *25*, 4992.
43. Tajima, K.; Yamada, Y.; Bao, S.; Okada, M.; Yoshimura, K. *Appl. Phys. Lett.* **2008**, *92*, 041912.